Applied Physics Letters

Opportunities and utilization of branching and step-out behavior in magnetic microswimmers with a nonlinear response

Cite as: Appl. Phys. Lett. **118**, 174102 (2021); https://doi.org/10.1063/5.0045454
Submitted: 26 January 2021 . Accepted: 31 March 2021 . Published Online: 27 April 2021

Felix Bachmann, Joshua Giltinan, Agnese Codutti, et al.

COLLECTIONS

Paper published as part of the special topic on Mesoscopic Magnetic Systems: From Fundamental Properties to Devices

This paper was selected as Featured

This paper was selected as Scilight

View Online Export Citation CrossMark

ARTICLES YOU MAY BE INTERESTED IN

Quirk of microswimmer propellers found to enable bimodal swimming and different applications
Scilight **2021**, 181103 (2021); https://doi.org/10.1063/10.0004931

Selectively controlled magnetic microrobots with opposing helices
Applied Physics Letters **116**, 134101 (2020); https://doi.org/10.1063/1.5143007

Magnetic nanohelices swimming in an optical bowl
Applied Physics Letters **119**, 012406 (2021); https://doi.org/10.1063/5.0058848

Challenge us.
What are your needs for periodic signal detection?
Watch

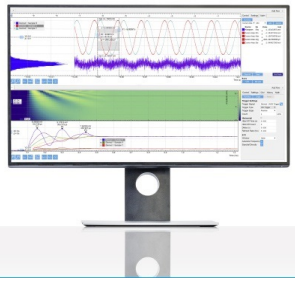

Zurich Instruments

© 2021 Author(s).

Applied Physics Letters ARTICLE scitation.org/journal/apl

Opportunities and utilization of branching and step-out behavior in magnetic microswimmers with a nonlinear response

Cite as: Appl. Phys. Lett. **118**, 174102 (2021); doi: 10.1063/5.0045454
Submitted: 26 January 2021 · Accepted: 31 March 2021 ·
Published Online: 27 April 2021

View Online Export Citation CrossMark

Felix Bachmann,[1] Joshua Giltinan,[2] Agnese Codutti,[1,3,a)] Stefan Klumpp,[3,4] Metin Sitti,[2,5,6] and Damien Faivre[1,7,b)]

AFFILIATIONS

[1]Max Planck Institute of Colloids and Interfaces, Department of Biomaterials, Am Mühlenberg 1, 14476 Potsdam, Germany
[2]Max Planck Institute for Intelligent Systems, Physical Intelligence Department, 70569 Stuttgart, Germany
[3]Max Planck Institute of Colloids and Interfaces, Department of Theory and Biosystems, Am Mühlenberg 1, 14476 Potsdam, Germany
[4]Institute for the Dynamics of Complex Systems, University of Göttingen, Friedrich-Hund-Platz 1, 37077 Göttingen, Germany
[5]Institute for Biomedical Engineering, ETH Zurich, 8092 Zurich, Switzerland
[6]School of Medicine and School of Engineering, Koc University, 34450 Istanbul, Turkey
[7]Aix-Marseille Université, CEA, CNRS, BIAM, 13108 Saint Paul lez Durance, France

Note: This paper is part of the APL Special Collection on Mesoscopic Magnetic Systems: From Fundamental Properties to Devices.
[a)]**Present address:** Technical University Munich, Department of Physics, James-Franck-Str. 1, 85748 Garching, Germany.
[b)]**Author to whom correspondence should be addressed:** damien.faivre@mpikg.mpg.de

ABSTRACT

Microswimmers are smart devices with potential applications in medicine and biotechnology at the micrometer-scale. Magnetic micropropellers with their remote control via rotating magnetic fields are especially auspicious. Helicoidal propellers with a linear velocity–frequency dependence emerged as the standard propulsion mechanism over the last decade. However, with their functions becoming more pivotal on the way to practical uses, deviations in shape and swimming behavior are inevitable. Consequently, propellers with nonlinear velocity–frequency relationships arise that not only pose different challenges but also offer advanced possibilities. The most critical nonlinearities are the wobbling behavior with its solution branching that has potential for bimodal swimming and the swimming characteristics in the step-out regime that are essential for selection and swarm control. Here, we show experimentally and with numerical calculations how the previously unpredictable branching can be controlled and, thus, becomes utilizable with an example 3D-printed swimmer device. Additionally, we report how two step-out modes arise for propellers with a nonlinear velocity–frequency dependence that have the potential to accelerate future microswimmer sorting procedures.

© 2021 Author(s). All article content, except where otherwise noted, is licensed under a Creative Commons Attribution (CC BY) license (http://creativecommons.org/licenses/by/4.0/). https://doi.org/10.1063/5.0045454

Microswimmers and especially remotely controlled magnetic microswimmers are envisioned for future biomedical applications and environmental remediation.[1–6] Over the last decade, a promising swimmer design has been widely studied: the so-called artificial bacterial flagella.[7–12] These helicoidally shaped swimmers possess a magnetization perpendicular to their long body axis that allows an externally applied magnetic field to stir them through fluids in a screw-like manner. In that case, the propulsion speed depends linearly on the actuation frequency.[8,9,11,13] Recently, the focus of research shifted toward functional applications of these microbots[14–19] that alter the surface composition and shape (e.g., propeller with and without a cargo). Thus, the previously utilized linear dependence between actuation frequency and propulsion velocity changes.[20] This can lead to traits such as tumbling, wobbling, and solution branching,[21–25] which are often viewed as deleterious for control (Fig. 1 illustrates these concepts schematically). However, these nonlinear characteristics can

© Author(s) 2021

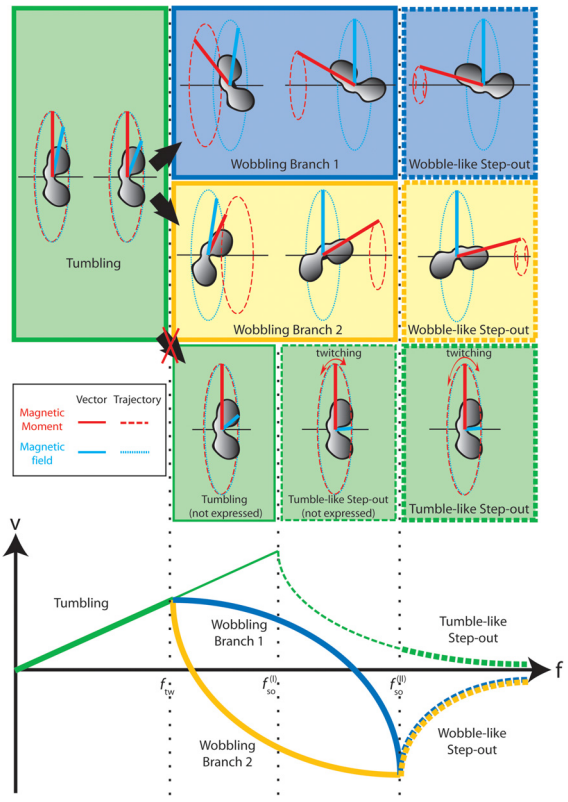

FIG. 1. Schematic illustration of nonlinear propeller dynamics. At low frequencies, a tumbling motion occurs (green "Tumbling" box), where the magnetic moment (red line) follows the externally applied field (light blue line) on a circular rotation. Increasing frequency only increases the angle between these two vectors. The result is a linear slope in the velocity–frequency graph (green bold line). At the transition frequency f_{tw}, two wobbling branches occur, where the propeller changes its rotation axis to decrease its rotational friction, and thus, the magnetic moment moves out of the magnetic field plane. There are two possible scenarios for this to happen (blue and yellow "Wobbling branch" boxes). Increasing frequency bow causes the propeller to rotate more and more around its long axis to further decrease its rotational friction. This process is energetically favorable compared to further following a tumbling motion with an increased angle between the magnetic moment and the magnetic field [bottom green "Tumbling (not expressed)" box]. At a certain frequency $f_{so}^{(I)}$, this not expressed tumbling behavior would result in a twitching step-out motion since the propeller can no longer follow the magnetic field through tumbling and the velocity would decrease, even for increasing field frequency [bottom green "Tumble-like step-out (not expressed)" box]. At a secondary step-out frequency $f_{so}^{(II)}$, it is not possible to maintain the hydrodynamic/magnetic torque balance, even for the wobbling solutions. As a result, a wobble-like step-out behavior occurs. As we show, the propeller rotates then on a trajectory with three-dimensional compensation loops (yellow and blue dashed boxes and lines). Additionally, we found that the tumble-like step-out behavior can also be expressed after $f_{so}^{(II)}$ (green dashed bold line). The above representations are only for illustration of the concepts. In practice, the transitions between the different phases are often more fluent and unstable branches might not be visible in experiments and simulations.

also have positive outcomes as they can be utilized for picking up or releasing cargo or drugs,[26] sensing,[27] changing swimming directions,[12,22,23,28] or the control of propeller swarms via their step-out behavior.[20,29–31] Step-out occurs above a certain frequency f_{so} and describes a nonlinear decline in propulsion velocity although the actuation frequency is increasing.[13,32,33] Overall, nonlinearity of the velocity–frequency dependence will become a more prominent challenge in future generation of magnetic micropropellers, however, a challenge that offers additional opportunities by utilizing these special characteristics.

Here, we characterize the nonlinear response of an example nonsymmetrical swimmer morphology both experimentally and with numerical hydrodynamic calculations. In our previous study, this morphology showed promise regarding the utilization as a frequency-controlled bidirectional microswimmer.[34] The dumbbell-shaped 4.5 μm long propellers are printed using a 3D lithography system and coated with a thin nickel layer that provides the magnetic moment ($|\vec{m}| \sim 10^{-14}$ A m^2) necessary for remote actuation via rotating magnetic fields and additionally a thin titanium layer for protection against oxidation (detailed characterization in Ref. 34). The size of this microswimmer is small enough to reach crucial targets in potential medical applications (red blood cell: ~6 μm), while it is large enough to mostly neglect Brownian motion and to be within the current limits of 3D-printing. First, the focus will be on influencing the occurring branching behavior, as it is in our view both the main challenge and the main opportunity when it comes to utilizing nonlinear magnetic micropropellers. Branching describes the existence of two swimming velocity responses (branches) at the very same actuation frequency caused by two different stable solutions for the propeller dynamics.[21,23,35] We show how a single shape in its branching regime can swim in two opposing directions by careful determination of the branch. In addition, we illustrate that this can be achieved either by strong constant magnetic fields that fix the initial orientations of the propellers before the actuation or by weak constant fields that are applied additionally to the rotating magnetic field. Furthermore, we show that two step-out behaviors exist, as was hinted previously by the observation of bistability of magnetic microhelices.[36,37] The two behaviors can be backtracked to the nonlinear regimes before the step-out frequency (tumbling and wobbling)[21,35,38] and the expected behavior can be qualitatively described by a simple theoretical model based on this connection. These findings will help utilizing the nonlinear characteristics, as those will be unavoidable for future generations of practical magnetic micropropellers since generating large quantities of microswimmers with the exact same properties will remain difficult.[34]

Our previous study on randomly shaped magnetic micropropellers suggests that nonlinearity of the velocity–frequency relationship and its branching in the wobbling regime is a common occurrence for magnetic micropropellers.[22,39] This is supported by our recent experimental study on 3D-printed microdevices[34] and that by Sachs *et al.*[40] on achiral microswimmers. These experimental findings are complemented by the theoretical work of Morozov *et al.*,[21,41] Meshkati and Fu,[23] and Cohen *et al.*,[28] which describes branching even for helicoidally shaped and achiral micropropellers. However, the experimental determination of the branching behavior remained untested until now. Additionally, step-out experiments were mostly performed for magnetic microswimmers with a linear velocity–frequency dependence[13,20,30,31,42] and precise examination for swimmers with nonlinear aspects is lacking.

Therefore, we utilized our previously produced 3D-printed propeller shape[34] that not only showed the desired nonlinearities for the velocity–frequency dependence (including solution branching) but also had additionally converse velocity responses in the branching

© Author(s) 2021

regime (schematic illustration in Fig. 1). Making these different responses accessible through branch determination shows promise for special microswimmer applications. Furthermore, this propeller shape has shown a low-velocity step-out behavior before,[34] which is crucial for selection control in propeller swarms and, hence, is studied in detail here.

The measured velocity–frequency behavior of the 3D-printed propeller is depicted by the combined data points in Fig. 2(a). After a nearly linear tumbling regime (1–15 Hz), the wobbling regime with two branches occurs (16–45 Hz). Here, for instance, at 35 Hz (dashed line), the propeller can swim in two different manners, with exactly the same external conditions applied (magnetic field strength, frequency, and rotation direction), only dependent on the solution branch. The two branch responses differ both in absolute velocity and in the overall swimming direction. Having a single velocity response makes the propeller control independent of its initial orientation; however, two velocity-responses (branches) at the same frequency offer additional possibilities when it comes to actuation schemes (e.g., in the case of limited accessible actuation frequencies). Here, we show two approaches to determine the branch a propeller follows, therefore offering a solution to the challenges mentioned above: (1) a strong constant magnetic field that determines the initial/starting conditions (SCs) before actuation and (2) a weak constant magnetic field that superposes the rotating field during actuation, where the sign of the constant field determines branching. For the first approach, three different starting conditions (SCs) are studied experimentally [Fig. 2(a)] and in simulations [Fig. 2(b)]. Details on the used simulations can be found in the supplementary material and in previous work.[34,39] The three constant fields are chosen in x-, positive and negative z-directions in the used lab frame (see the supplementary material, Fig. S2). The rotation axis of the afterward applied rotating field is around the positive z-axis. This means that, before actuation, the magnetic moment fixed in the microproppeller will align perpendicular to the said axis (SC1, typical standard for magnetic microproppeller measurements) and parallel and antiparallel (SC2 and SC3), respectively. For SC1 $\vec{m}\uparrow\uparrow\vec{x}$ is the magnetic moment in the plane of rotation when an external rotating field is applied; for SC2 $\vec{m}\uparrow\uparrow\vec{z}$ is the magnetic moment aligned parallel to the axis of rotation; for SC3 $\vec{m}\uparrow\downarrow\vec{z}$ is the magnetic moment aligned antiparallel to the axis of rotation.

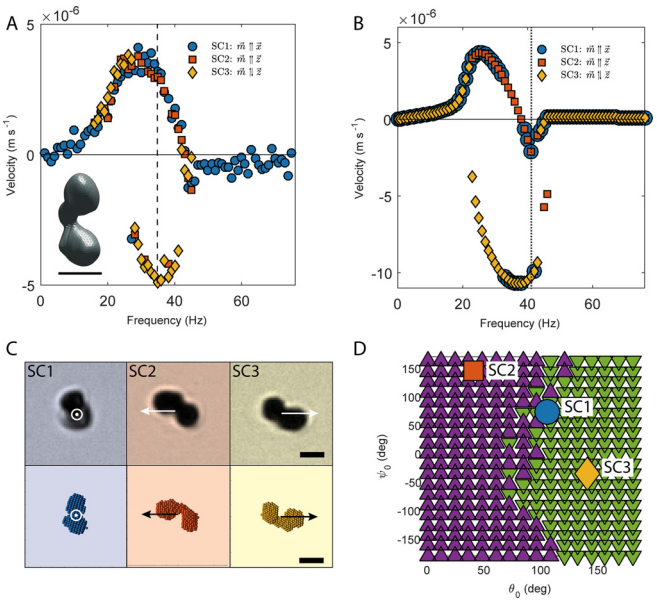

FIG. 2. Influencing the branching behavior through different starting conditions. (a) A 3D-printed propeller was measured with three different starting conditions SC1-3 experimentally. The inset shows the 3D-model of the propeller. Scale bar = 2 μm. (b) The simulated data qualitatively agree with the experimental data, showing different branching distribution (between $f \approx 16$ to 45 Hz) for the respective starting conditions. (c) Starting conditions in experiments (top) and simulations (bottom) are illustrated in the optical images and bead-based representations, respectively. Scale bar = 2 μm. (d) Dependency of branching on the starting values θ_0 and ψ_0 at $f = 41$ Hz (dotted line in b): purple upward-pointing triangles represent the continuous upper branch (higher velocity) and green downward-pointing triangles the secondary lower branch (lower velocity). The three chosen starting conditions are represented by their respective symbol from the main plot (a/b). SC1 is in an area where small deviations in the starting orientation can result in a switching of the branching, whereas this is not the case for SC2 and SC3.

Figure 2(a) shows three measurements with the same propeller but with the three different starting conditions (SC1-3). The blue circles show SC1 between 1 and 75 Hz, which serves here as a reference measurement. SC2 and SC3 (red squares and yellow diamonds, respectively) are only shown in the branching regime between 16 and 45 Hz. Depending on the starting condition, the distribution of measured velocity points changes with respect to the actuation frequency. Aligning the propeller perpendicular to the z-axis (SC1) before the rotating field is applied mostly populates the continuous upper branch.[21] The same applies for an initial alignment of the propeller parallel to the z-axis (SC2). However, aligning it antiparallel (SC3) mostly populates the lower branch. A similar picture emerges for the respective numerical simulations in Fig. 2(b) (cf. see the supplementary material, Table S1, Sim1). The accordant starting conditions for both experiments and simulations are illustrated in Fig. 2(c). In these simulations, the starting conditions can be expressed by two angles, θ_0 and ψ_0 (polar and azimuthal angle, see the supplementary material, Fig. S2). These Euler angles describe how the body coordinate system (BCS) is oriented in the lab coordinate system (LCS).

Different values for these angles will result in different initial orientations of the propeller in the externally applied field. Similar to spherical coordinates, θ_0 and ψ_0 can be varied from 0 to 180° and −180° to +180°, respectively, to sample different spherical orientations of the propeller in the LCS. Depending on this initial orientation, the propeller will follow either of the two possible branch behaviors (here indicated as the "upper" and "lower" branch due to the difference in relative velocity at the applied frequency). Plotting this branch assignment over different value pairs of θ_0 (in 12° steps) and ψ_0 (in 18° steps) illustrates the dependence of branching on the starting conditions [Fig. 2(b), for $f = 41$ Hz, cf. see the supplementary material, Table S1, Sim2]. The values of SC1 (blue dot) show a data point directly in the contact zone of the two branches. In experiments, thermal fluctuations and other disturbances can slightly change the starting conditions and the branch assignment becomes unsure. SC2 (red square) lies well inside the upper branch phase (purple upward-pointing triangles), and SC3 (yellow diamond) lies well inside the lower branch phase (green downward-pointing triangle). Small deviations from SC2 and SC3 should not change the branch assignment, making the branching behavior more controllable. These theoretical findings strongly support the experimental results and suggest that an

© Author(s) 2021

initial orientation of the propeller similar to one of its branching configuration during rotation[21,22] confines the propeller to this branch.

The second approach to influencing branch assignment is to keep a small constant field component ($B_1 \ll B_0 = 1$ mT) even during the field rotation. The effective magnetic field vector then describes a flat cone: $\vec{B}(t,\omega) = (B_0\cos(\omega t), B_0\sin(\omega t), B_1)$. Again, three cases were tested: (i) $B_1 = 0$ mT (as reference); (ii) $B_1 = +0.1$ mT; (iii) $B_1 = -0.1$ mT. The starting conditions SC1-3 were still applied for the three cases, respectively. The experimental results of another 3D-printed sample propeller are shown in Fig. 3(a) (v–f-diagram in 5 Hz steps), and the according numerical simulation results are shown in Fig. 3(b) (v–f-diagram in 1 Hz steps, cf. see the supplementary material, Table S1, Sim3). Both graphs show no clear determination of the branches for $B_1 = 0$ and SC1 (blue dots). For $B_1 \neq 0$, the propeller behavior splits into two distinct branches (yellow diamonds and red squares), with a striking qualitative agreement between experiments and simulations. The additional constant magnetic field component slightly alters the axis of rotation and, therefore, the rotation behavior, in both the linear tumbling regime and in the following wobbling regime. With the small constant field adjustment, a reproducible

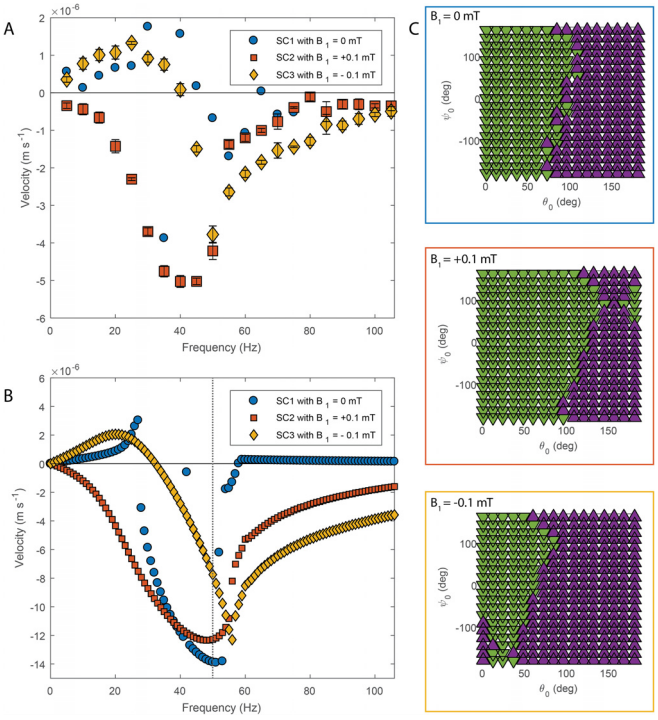

FIG. 3. Controlling propeller behavior by an additional constant field component. (a) Experimental measurement using an additional constant field of $B_1 = +0.1$ mT and $B_1 = -0.1$ mT (red squares and yellow diamonds, respectively, standard error of the mean with n = 3). As a reference, the same propeller was measured without a constant field component (blue circles, $B_1 = 0$ mT). (b) Simulations under equivalent conditions show qualitative agreement, not only in branching determination but also in the general deviation from the reference case ($B_1 = 0$ mT). (c) Phase diagram of branch assignment over the starting condition. In simulations, additional field components shift the border between the branch phases, increasing the probability for the respective case ("upper branch": purple upward-pointing triangles; "lower branch": green downward-pointing triangles; at $f = 50$ Hz, dotted line in b).

branch assignment was possible, even experimentally ($n = 3$). The calculated phase diagrams of starting conditions and branch assignment are shown in Fig. 3(c) (at $f = 50$ Hz) for the three cases (cf. see the supplementary material, Table S1, Sim4). As can be expected, for $B_1 = 0$ mT, about half of the tested propeller orientations lead to the upper branch behavior, while the other half leads to the lower branch. However, additional field components shift this balance to favor either the lower branch ($B_1 = +0.1$ mT: green downward-pointing triangles) or the upper branch ($B_1 = -0.1$ mT: purple upward-pointing triangles). Therefore, the phase border of the respective branch is already shifted by small constant field components. This makes a clear branch determination and predictable behavior possible.

The second nonlinear characteristic that offers unused potential for magnetic microswimmers is the step-out behavior at high rotation frequencies. This behavior is neglected in many experimental and theoretical studies. Reasons are that the velocity decreases in this regime, making it inefficient for propulsion, and additionally, a simple theoretical description is only accessible for one specific case.[13,32,33] However, this nonlinear regime plays a crucial role in selection, sorting, and swarm control.[20,29–31,43] Therefore, we decided to thoroughly characterize this region of the velocity–frequency relationship for the exemplary propeller. Our results show that not only two configurations for this step-out behavior are generally possible, but also they can occur for the same propeller. Figure 4(a) shows image sequences recorded at 50 frames per second (fps) of the same propeller beyond $f_{so} \approx 45$ Hz. A tumble-like step-out behavior (rotation around the short propeller axis) occurs with a long period ($T \approx 0.18$ s: top, yellow, at $f = 61$ Hz). A wobble-like step-out behavior (rotation around the long propeller axis) occurs with a short period ($T \approx 0.07$ s: bottom, red, at $f = 62$ Hz). This means that a full rotation of the propeller around the short axis (here termed the period) takes significantly longer, indicating more back and forth twitching, compared to the rotation around the long propeller axis, even though the applied external frequency is similar. As a result, the reduced effective rotation frequency[13,32] differs heavily, depending on the trait: $f_{eff} \approx 5.56$ Hz for the tumble-like step-out behavior and $f_{eff} \approx 14.29$ Hz for the wobble-like step-out behavior. Similar to the wobbling branching, the assignment toward one solution was not fixed in repeated measurements but relies again on the initial propeller configuration (cf. see the supplementary material, Fig. S4). The tumble-like step-out behavior already occurred in our previous study with randomly shaped micropropellers, while a wobble-like step-out behavior resembles that of a helical propeller. Based on the experimental data (see the supplementary material, Fig. S4), both gaits could be found in simulations by adjusting again the starting configuration of the propeller to be similar to the respective step-out solution (cf. see the supplementary material, Table S1, Sim5). The results can be seen in Fig. 4(b) with yellow diamonds for the tumble-like solution and red squares for the wobbling solution. The bead-based representations in the respective colors illustrate the different configurations and are comparable with the optical microscopy images in Fig. 4(a). Additional to the simulation data, a theoretical model is included. This model follows the analytical solution for the step-out behavior of linear magnetic microswimmers[13,32,33] with $v = c \cdot (f - \sqrt{f^2 - f_{so}^2})$ and adapts to the adequate step-out frequencies f_{so} and coupling coefficients c. Therefore, the step-out frequencies for the tumbling and wobbling regime are considered,[35,37] here termed $f_{so}^{(I)}$ and $f_{so}^{(II)}$, respectively, and marked in the plot of Fig. 4(b). The coupling

© Author(s) 2021

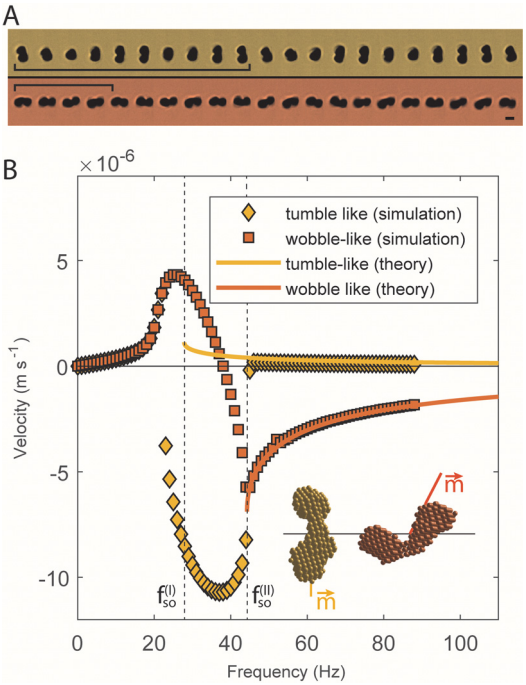

FIG. 4. Two step-out behaviors. (a) Microscope image sequence (50 fps) showing two different behaviors above step-out frequency: tumble-like (yellow, top, at 61 Hz) and wobble-like (red, bottom, at 62 Hz). Scale bar: 2 μm. The full-turn period of the tumble-like behavior is much longer than that for the wobble-like case. (b) Numerical simulations showing these two behaviors (red squares and yellow diamonds and bead-based representations of the respective configuration) with an approximate theory (solid lines).

coefficient ($c = v/f$) for the tumble-like step-out behavior was extracted from the linear tumbling regime ($c^{(I)} \approx 0.41 \times 10^{-7}$ μm), while for the nonlinear wobbling-like step-out, the last coupling coefficient at $f_{so}^{(II)}$ was taken ($c^{(II)} \approx 1.56 \times 10^{-7}$ μm).

Although the agreement between simulations and theory fits well in this case, these models are not generally applicable, as they assume the limiting case of a linear-propeller-like step-out behavior. Details on the differences between the two step-out behaviors can be found in the supplementary material.

The complex tasks for the envisioned future biomedical and environmental applications will require sophisticated microswimmers that do not only swim but also fulfill other tasks such as cargo transport, drug delivery, and environmental cleaning. It is therefore foreseeable that future microswimmer generations will benefit from a broader design space than the current mostly helical shapes with the main goal of swimming fast.[7,9,41,44] However, advanced shapes will alter the swimming behavior, and nonlinear characteristics (such as solution branching) need to be considered. Yet, these nonlinearities can not only be seen as a challenge but also as an opportunity for alternative actuation schemes. We illustrate the selection of a designated branch by controlling initial orientation of the micropropeller or by altering the actuation field to have a bias for one or the other branch. These results agree well with theoretical findings by Meshkati and Fu[23] and more recently by Cohen *et al.*[28] that show how conical actuation fields can lead to bistability and direction control. Similar to what Meshkati and Fu theoretically saw, we observed stable solutions only for small constant components ($B_1/B_0 \sim 0.1$). Additionally, the behavior shown in Fig. 3 agrees nicely with the results for achiral propellers in the study by Cohen *et al.*,[28] which could be explained by the roughly symmetric dumb-bell shape of the here considered propeller.

Furthermore, we show two distinct step-out modes that can help for faster selective swarm control than is currently the case[12,20,29–31] by employing the rapid velocity drop off in a narrow frequency window. Using magnetic gradients to have special selective starting conditions could enable this in medical imaging techniques such as magnetic resonance imaging (MRI) or magnetic particle imaging (MPI) that already utilize such fields. Similarly, this technique could be used to access different swimming modes by utilizing branching (e.g., swimming/non-swimming mode, changing direction, and increasing/decreasing velocity without changing frequency). These findings can enable alternative concepts for employing single micropropellers and, more importantly, allow us to actuate and control many propellers at the same time, which is a crucial step for the practicability in future applications.

See the supplementary material for experimental and simulation details.

This work was funded by the Max Planck Society and was supported by the Deutsche Forschungs-gemeinschaft within Priority Program 1726 on microswimmers (Grant Nos. FA 835/7-1 and KL 818/2-1).

DATA AVAILABILITY

The data that support the findings of this study are available from the corresponding author upon reasonable request.

REFERENCES

[1]J. Wang and W. Gao, ACS Nano **6**, 5745 (2012).
[2]H. Ceylan, J. Giltinan, K. Kozielski, and M. Sitti, Lab Chip **17**, 1705 (2017).
[3]K. Bente, A. Codutti, F. Bachmann, and D. Faivre, Small **14**, 1704374 (2018).
[4]S. Klumpp, C. T. Lefèvre, M. Bennet, and D. Faivre, Phys. Rep. **789**, 1 (2019).
[5]H. Ceylan, I. C. Yasa, U. Kilic, W. Hu, and M. Sitti, Prog. Biomed. Eng. **1**, 012002 (2019).
[6]M. Sitti, *Mobile Microrobotics* (MIT Press, Cambridge, MA, 2017).
[7]L. Zhang, J. J. Abbott, L. Dong, B. E. Kratochvil, D. Bell, and B. J. Nelson, Appl. Phys. Lett. **94**, 064107 (2009).
[8]L. Zhang, J. J. Abbott, L. Dong, K. E. Peyer, B. E. Kratochvil, H. Zhang, C. Bergeles, and B. J. Nelson, Nano Lett. **9**, 3663 (2009).
[9]A. Ghosh and P. Fischer, Nano **9**, 2243–2245 (2009).
[10]B. Behkam and M. Sitti, J. Dyn. Syst. Meas. Controlled Trans. ASME **128**, 36 (2006).
[11]S. Tottori, L. Zhang, F. Qiu, K. K. Krawczyk, A. Franco-Obregõn, and B. J. Nelson, Adv. Mater. **24**, 811 (2012).
[12]J. Giltinan, P. Katsamba, W. Wang, E. Lauga, and M. Sitti, Appl. Phys. Lett. **116**, 134101 (2020).
[13]D. Schamel, M. Pfeifer, J. G. Gibbs, B. Miksch, A. G. Mark, and P. Fischer, J. Am. Chem. Soc. **135**, 12353 (2013).
[14]F. Qiu, S. Fujita, R. Mhanna, L. Zhang, B. R. Simona, and B. J. Nelson, Adv. Funct. Mater. **25**, 1666 (2015).
[15]M. Hoop, Y. Shen, X. Z. Chen, F. Mushtaq, L. M. Iuliano, M. S. Sakar, A. Petruska, M. J. Loessner, B. J. Nelson, and S. Pané, Adv. Funct. Mater. **26**, 1063 (2016).
[16]C. Peters, M. Hoop, S. Pané, B. J. Nelson, and C. Hierold, Adv. Mater. **28**, 533 (2016).

© Author(s) 2021

[17]J. Li, B. E. F. De Ávila, W. Gao, L. Zhang, and J. Wang, Sci. Robot. **2**, eaam6431 (2017).
[18]H. Ceylan, I. C. Yasa, O. Yasa, A. F. Tabak, J. Giltinan, and M. Sitti, ACS Nano **13**, 3353 (2019).
[19]I. C. Yasa, A. F. Tabak, O. Yasa, H. Ceylan, and M. Sitti, Adv. Funct. Mater. **29**, 1808992 (2019).
[20]X. Wang, C. Hu, L. Schurz, C. De Marco, X. Chen, S. Pané, and B. J. Nelson, ACS Nano **12**, 6210 (2018).
[21]K. I. Morozov, Y. Mirzae, O. Kenneth, and A. M. Leshansky, Phys. Rev. Fluids **2**, 044202 (2017).
[22]F. Bachmann, K. Bente, A. Codutti, and D. Faivre, Phys. Rev. Appl. **11**, 34039 (2019).
[23]F. Meshkati and H. C. Fu, Phys. Rev. E **90**, 063006 (2014).
[24]H. C. Fu, M. Jabbarzadeh, and F. Meshkati, Phys. Rev. E **91**, 043011 (2015).
[25]U. K. Cheang, F. Meshkati, D. Kim, M. J. Kim, and H. C. Fu, Phys. Rev. E **90**, 033007 (2014).
[26]A. Barbot, D. Decanini, and G. Hwang, Sci. Rep. **6**, 19041 (2016).
[27]A. Ghosh, D. Dasgupta, M. Pal, K. I. Morozov, A. M. Leshansky, and A. Ghosh, Adv. Funct. Mater. **28**, 1705687 (2018).
[28]K. J. Cohen, B. Y. Rubinstein, O. Kenneth, and A. M. Leshansky, Phys. Rev. Appl. **12**, 01402 (2019).
[29]P. J. Vach, S. Klumpp, and D. Faivre, J. Phys. D: Appl. Phys. **49**, 65003 (2015).
[30]T. A. Howell, B. Osting, and J. J. Abbott, Phys. Rev. Appl. **9**, 54021 (2018).
[31]A. W. Mahoney, N. D. Nelson, K. E. Peyer, B. J. Nelson, and J. J. Abbott, Appl. Phys. Lett. **104**, 144101 (2014).
[32]P. J. Vach, P. Fratzl, S. Klumpp, and D. Faivre, Nano Lett. **15**, 7064 (2015).
[33]A. Cebers and M. Ozols, Phys. Rev. E **73**, 021505 (2006).
[34]F. Bachmann, J. Giltinan, A. Codutti, S. Klumpp, M. Sitti, and D. Faivre, Adv. Intell. Syst. **2**, 2000078 (2020).
[35]K. I. Morozov and A. M. Leshansky, Nanoscale **6**, 1580 (2014).
[36]A. Ghosh, D. Paria, H. J. Singh, P. L. Venugopalan, and A. Ghosh, Phys. Rev. E **86**, 031401 (2012).
[37]A. Ghosh, P. Mandal, S. Karmakar, and A. Ghosh, Phys. Chem. Chem. Phys. **15**, 10817 (2013).
[38]Y. Man and E. Lauga, Phys. Fluids **25**, 071904 (2013).
[39]A. Codutti, F. Bachmann, D. Faivre, and S. Klumpp, Front. Robot. **AI 5**, 109 (2018).
[40]J. Sachs, K. I. Morozov, O. Kenneth, T. Qiu, N. Segreto, P. Fischer, and A. M. Leshansky, Phys. Rev. E **98**, 063105 (2018).
[41]Y. Mirzae, O. Dubrovski, O. Kenneth, K. I. Morozov, and A. M. Leshansky, Sci. Robot. **3**, eaas8713 (2018).
[42]P. J. Vach, N. Brun, M. Bennet, L. Bertinetti, M. Widdrat, J. Baumgartner, S. Klumpp, P. Fratzl, and D. Faivre, Nano Lett. **13**, 5373 (2013).
[43]P. Katsamba and E. Lauga, Phys. Rev. Appl. **5**, 064019 (2016).
[44]E. E. Keaveny, S. W. Walker, and M. J. Shelley, Nano Lett. **13**, 531 (2013).

© Author(s) 2021